JOURNAL OF MATERIALS RESEARCH AND TECHNOLOGY 2023;24:1015–1033

Available online at www.sciencedirect.com

jmr&t Journal of Materials Research and Technology

journal homepage: www.elsevier.com/locate/jmrt

Original Article

Aloe vera silver nanoparticles addition in chitosan films: improvement of physicochemical properties for eco-friendly food packaging material

Valeria De Matteis [a,b,*], *Mariafrancesca Cascione* [a,b,**], *Daniele Costa* [a], *Simona Martano* [a], *Daniela Manno* [a], *Alessandro Cannavale* [c], *Stefano Mazzotta* [d], *Fabio Paladini* [a], *Maurizio Martino* [a], *Rosaria Rinaldi* [a,b]

[a] *Department of Mathematics and Physics "Ennio De Giorgi", University of Salento, Via Arnesano, 73100 Lecce (LE), Italy*

[b] *Institute for Microelectronics and Microsystems (IMM), CNR, Via Monteroni, Lecce, 73100, Italy*

[c] *Dipartimento di Architettura, Costruzione e Design, Politecnico di Bari, Via Orabona 4, Bari, 70125, Italy*

[d] *Studio Effemme-Chimica Applicata, Via Paolo VI, 73018 Squinzano (LE), Italy*

ARTICLE INFO

Article history:
Received 17 October 2022
Accepted 5 March 2023
Available online 14 March 2023

Keywords:
Chitosan Films
Green AgNPs
Physicochemical properties
Food packaging

ABSTRACT

In recent times, the searches for alternative materials to plastic is a popular topic, due to the danger that synthetic materials cause to the environment and humans. Among the promising natural polymers, chitosan (CS) is certainly one of the most suitable since it it is edible, non-toxic and derives from crustacean waste.- However, it is necessary to improve its physical properties to be widely applied in food packaging, whose market is dominated by synthetic plastic. In this work we have synthesized silver nanoparticles (AgNPs) using hot-plate and microwaves-based techniques, using *Aloe Vera* leaves extracts. The synthetic process follows the principles of green chemistry, since no toxic substance is used to obtain nanomaterials. These NPs, having dimensions <20 nm, were characterized by TEM, zeta potential, UV–vis, FTIR, and then added to CS having low and medium molecular weight to develop thin films after its polymerization. These films were evaluated in terms of swelling ratio, optical properties, thermal stability, wettability, roughness, and friction coefficient, understanding that the physical properties of the films improved after the intercalation of the AgNPs, albeit differences were observed using the two NPs type. Subsequently, the release of silver ions from films using different pH as well as *in vitro* toxicity tests were carried out to evaluate their applicability. Largely, the excellent properties of new composite materials make them promising materials for packaging of different kinds of foods.

* Corresponding author. Department of Mathematics and Physics "Ennio De Giorgi", University of Salento, Via Arnesano, 73100 Lecce (LE), Italy

** Corresponding author. Department of Mathematics and Physics "Ennio De Giorgi", University of Salento, Via Arnesano, 73100 Lecce (LE), Italy

E-mail addresses: valeria.dematteis@unisalento.it (V. De Matteis), mariafrancesca.cascione@unisalento.it (M. Cascione).

https://doi.org/10.1016/j.jmrt.2023.03.025

1. Introduction

Synthetic polymers with a large molecular mass, usually referred to as "plastics", appear to be mighty materials due to their tunable excellent chemical–physical properties, which make them highly versatile in several application fields. In general, they derive from petroleum oil [1] and the best-known synthetic polymers are polyamides (nylon), Poly (vinylchloride) (PVC), Polystyrene (PS), Polytetrafluoroethylene (PTFE), Teflon, Polyethylene (PE), epoxy, and synthetic rubbers [2]. However, the chemical reactions used to produce synthetic polymers are highly exothermic; in addition their low biodegradability can have adverse on environment due to their accumulation without the possibility to recycle [3–5]. For these reasons, the current challenge is the search of biocompatible materials having similar characteristics to synthetic plastics in order to build a new era based on the eco-friendly materials following the principle of green chemistry and circular economy [6,7]. To date, biopolymers turn out to be the best candidates for synthetic plastic replacement [8]; in this context, natural polysaccharides are particularly fascinated for their non-toxic behavior, biodegradability, and availability in large quantities [9,10]. Chitosan (CS) represents a promising alternative to plastic in several applications. CS is a chitin deacetylation product constituted of glucosamine and N-acetylglucosamine linked by (1–4) glycosidic bonds [11]. It is soluble in acidic solutions and its molecular weight influences its own excellent film forming properties, making it suitable for many kinds of applications in food, chemical industry and biomedical devices [12]. However, some concerns were raised regarding the high wettability, low stiffness and high transmittance values make it unsatisfactory to use it in the food field [13]. To overcome these drawbacks, the scientific community moved to incorporate some types of fillers able to improve CS physicochemical properties [14,15]. For example, ZnO nanoparticles (ZnONPs) dispersed in Polylactic Acid (PLA) matrix reduce the permeability coefficients of oxygen (PO_2) and carbon dioxide (PCO_2), by 18% and 17%, respectively [16]; Graphene [17], PEG [18], TiO_2NPs [19] and other nanomaterials were used to tune the properties of chitosan films, in particular the antibacterial activity. The employment of NPs represents one of the most promising solution due to the possibility of engineering their properties simply modulating their shape and size or functionalizing the surface by specific molecules [20]. However, the chemical routes commonly used to produce NPs, especially metallic NPs, are time-consuming and employ toxic substances as reducing and capping agents [21]. For these reasons, their incorporation into CS films might be inappropriate for food packaging applications for possible food contamination. Furthermore, disposal could be complicated, making difficult the safe recycling. Then, the development of green approaches to achieve NPs, in which only natural compounds are employed, is important with the aim to incorporate in the chitosan film only safe NPs [22–24].

In this work, we used two different green routes to obtain silver NPs (AgNPs), using leaves extract of *Aloe Vera*. This plant is widely spread in the Mediterranean area and it is extensively applied in the agricultural, biomedical, and cosmetic fields [25]. In the last case, in particular, the gel contained in leaves is a precious material typically used to produce skin and beauty lotions [26]. Instead, the epidermis of the leaf is a waste but, since it contains high concentrations of vitamins, proteins, and polyphenols [27,28] its extract can be used to obtain AgNPs. The plant extract acting as reducing and capping agent through two different protocols, respectively based on the use of hot-plate and microwaves (MW). The obtained AgNPs were carefully characterized by Transmission Electron Microscopy (TEM), Inductively Coupled Plasma Atomic Emission Spectrometry (ICP-AES), Potential-ζ, UV–vis and FTIR spectroscopies. Then, they were subsequently added in CS having low (50–190 kDa), and medium molecular weight (190–310 kDa). The surface properties of the nanocomposite films were analyzed by Atomic Force Microscopy (AFM) and contact angle to obtain information about roughness and wettability, respectively. Then, the swelling behavior, the transmittance and thermal properties were investigated as well as their toxicity *in vitro* and silver ions (Ag^+) release in different pH buffers to test their safeness. Our result demonstrated that the AgNPs achieved by MW induced great improvement of CS films compared to NPs obtained by hot-plate-based protocol. Hence, these kind of nanocomposite films appeared to be the best candidate for use in the food industry as packaging materials.

2. Materials and methods

2.1. Green synthesis of AgNPs

2.1.1. Preparation of leaves extracts

Aloe vera leaves were kindly donated from the company "*Natural is better*" (Martano, Lecce, Italy), washed with MilliQ to eliminate pollution and dried at room temperature for one day. Then, 10 g of leaves were cut and transferred into a glass flask containing 100 mL of MilliQ water. The solution was boiled at 100 °C for 20 min and after cooling, it was filtered by a cellulose membrane (Whatman n.1) before use.

2.1.2. Green AgNPs by hot-plate procedure

5 mL of leaves extract was added to 50 mL of $AgNO_3$ (1 mM) and heated at60 °C for 45 min. During this time, the reaction color switched from light yellow to brown indicating the

chemical reduction of Ag^{+} ions into Ag^{0} (pH 7). Finally, the solution was centrifuged at 4000 rpm for 1 h to collect NPs. The latter were stored in the dark at 4 °C.

The schematic representation of procedure was reported in Fig. 1a.

2.1.3. *Green AgNPs by MW procedure*

The synthesis of AgNPs by MW was performed using 9 mL of $AgNO_3$ solution (1 mM) and 100 μL of *Aloe Vera* leaves extract. Several experimental tests were performed by modifying two variables.

- reaction times (60 ÷ 360) s;
- the power of the microwave oven (119 ÷ 700) W.

The formation of AgNPs was ensured by the visible color change using a power of 375 W for 4 min in the microwave oven. After this step, the solution was centrifuged at 13,000 rpm for 15 min to obtain AgNPs in the pellet. Further centrifugation steps were carried out to eliminate any organic residues. The obtained NPs were stored at 4 °C prior to characterization. The schematic representation of the procedure was showed in Fig. 1b.

2.2. *Characterization of green Ag NPs*

2.2.1. *Transmission Electron Microscopy (TEM) analysis*

Structural, morphological analyses and Selected Area Electron Diffraction (SAED) patterns were performed by Hitachi 7700 Transmission Electron Microscope (Hitachi High-Tech, Tokyo, Japan), operating at 100 kV; 10 μL of the two different AgNP solutions was dropped onto standard 400-mesh carbon-supported copper grids and air-dried overnight. Statistical analysis of AgNPs size was obtained by particle analysis plugin in ImageJ software (National Institutes of Health, United States (USA)).

2.2.2. *Dynamic light scattering (DLS) and ζ-potential analyses*

The DLS and ζ-potential measurements of green AgNPs were recorded by means Zetasizer Nano-ZS, equipped with a HeNe laser (4.0 mW) working at 633 nm detector (ZEN3600, Malvern Instruments Ltd., Malvern, UK) in aqueous solutions (25 °C, pH 7).

2.2.3. *UV–vis analysis*

The absorption spectra (in the spectral range 300 ÷ 800 nm) of the green Ag NPs were measured with a Cary 300 UV–vis spectrophotometer (Varian, Palo Alto, CA, United States (USA)) at a resolution of 1 nm using a 5-mm path length quartz cuvette.

2.2.4. *Fourier transform infrared (FTIR) spectroscopy*

Jasco-670 Plus FTIR spectrometer (Jasco, Tokyo, Japan) was used to measure the FTIR spectra over a range of 800 ÷ 4000 cm^{-1} of the two types of Ag NPs, at a resolution of 4 cm^{-1}.

2.2.5. *NPs concentration*

The concentrations of the green Ag NPs were calculated by elemental analyses using ICP-OES (PerkinElmer AVIO 500). 250 μL of the NPs solutions were digested overnight by adding 2 mL of nitric acid (HNO_3), followed by dilution with MilliQ water (1:5).

2.3. *Preparation of green AgNPs based-chitosan films and characterization*

2.3.1. *Green AgNPs addition in chitosan solution*

2% w/v of CS films were prepared by dissolving 200 mg of polymer (powder) in 10 mL of acetic acid 1%. Two different types of CS were used for this purpose: CS low molecular weight (Sigma–Aldrich, Dorset, UK, 50–190 kDa) and CS

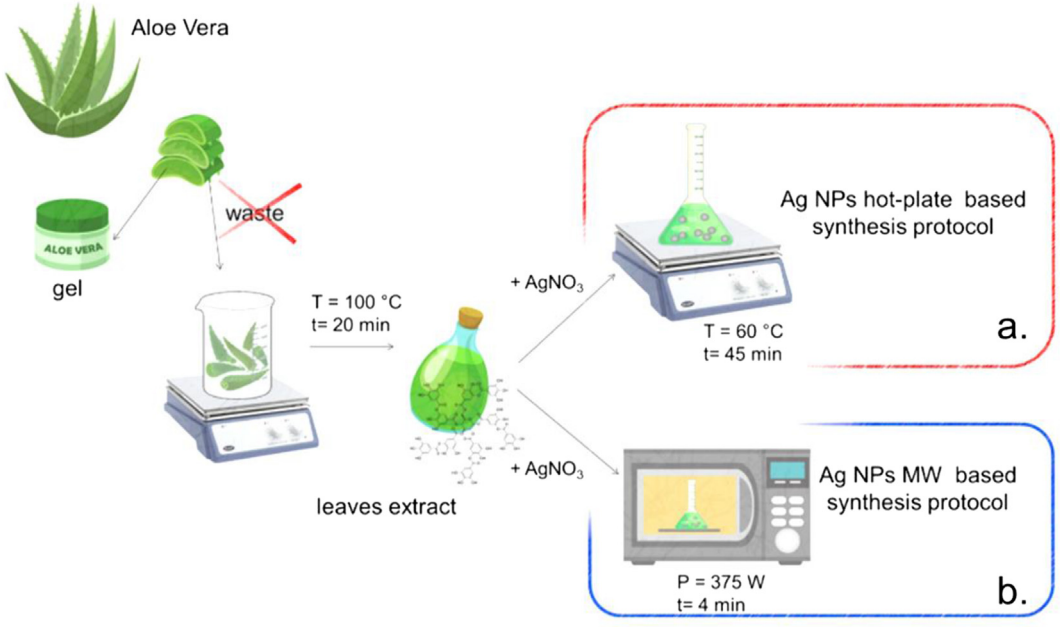

Fig. 1 – Graphical representation of AgNPs achieved by hot-plate and microwave assisted methods.

medium molecular weight (Sigma–Aldrich, Dorset, UK, 190–310 kDa) with the same degree of deacetylation (75–85%). The green AgNPs obtained by the two different synthetic approaches previously described, were added in CS low and medium to obtain the final concentrations of 60 μM and 120 μM. CS solutions (3 mL) were deposited by drop casting in polystyrene *Petri* dishes (diameter 35 mm) and left to polymerize under hood for 24 h at room temperature.

The prepared samples were.

- CS Low 2% and CS Med 2%, corresponding to the CS samples without NPs. They were used as control samples.
- CS Low 60, CS Low 120, CS Med 60 and CS Med 120, corresponding to the films with 60 μM and 120 μM of AgNPs produced by hot-plate-based synthesis.
- CS Low MW 60, CS Low MW 120, CS Med MW 60 e CS Med MW 120, corresponding to the films achieved adding 60 μM and 120 μM of AgNPs obtained by MW-based protocol.

2.4. Chitosan films characterization

2.4.1. Swelling ratio study

The swelling experiments carried out on the CS films and CS-based NPs (hot-plate and MW) at two concentrations were performed in water at 25 °C and 37 °C (pH 7.0). Each sample, i.e. pure CS films (low and medium), CS Low 60, CS Low 120, CS Med 60 and CS Med 120 with AgNPs achieved by hot-plate and MW, were weighed by analytical balance after vacuum drying. t = 0 represented the time in which the samples were immersed in water; then, films were removed from water at t = 60, 120 and 180 min, dried and weighted.

The swelling percentage (S %) was calculated by the following equation:

$$S\,\% = \frac{W_t - W_0}{W_0} * 100$$

where S%, W_t and W_0 were the swelling percent, weight at different time points and initial weight of the film, respectively.

2.4.2. Transmittance measurements

Transmittance spectra of the self-standing membranes were measured using a Perkin–Elmer spectrophotometer (UV–Vis–NIR) in a wavelength range spanning from 200 nm to 900 nm.

2.4.3. Wettability analysis by contact angle measurements

The wettability was evaluated through the contact angle measurements performed using the sessile drop technique. The experimental set-up consists of a high chamber Speed Redlake Imaging Motion Scope (DEL imaging, Woodsville, NH, USA), a linear positioner (Holmark, Kalamassery, Kerala, India) with tilting table integrated, a backlit LED diffuser (Edmund, Reno, NV, USA) with control intensity and a microliter drop dispenser module (Hamilton, York, UK). The measurements were made at temperature of (21.5 ± 0.5) °C and relative humidity of (57 ± 5) %, by depositing a drop (≃ 2.5 μL) of distilled water. Droplet deposition was recorded by frame grabber system from transient phase to steady-state configuration in which the static contact angle was measured. Five measurements for each sample were performed The images were processed using ImageJ v1.53 k software (National Institutes of Health, USA) using "Drop Shape Analysis" plugin in the mode LB-ADSA (Low-Bond Axisymmetric Drop Shape Analysis).

2.4.4. Roughness analysis by Atomic Force Microscopy (AFM)

The experiments were performed using AFM (Bioscope Catalyst, Bruker Inc., Santa Barbara, CA, USA), implemented on an optical microscope inverted (Zeiss Observer Z1, Zeiss, Jena, Germany). The entire system is positioned on an insulating base to minimize the effects due to environmental mechanical vibrations during acquisitions. HarmoniX Microlever (HMX, Bruker Inc., USA) tip, consisting of a cantilever with a rectangular geometry of silicon doped with antimony, having a nominal stiffness of 4 N/m, was used to perform AFM measurements. For each sample, the scans were carried out on an area of 20*20 μm at 512 (lines) x 512 (dots) resolution. These acquisitions were analyzed through the NanoScope Analysis software (Bruker Inc., USA) to quantify the parameter of roughness, expressed as Rq (root-mean-square roughness):

$$R_q = \sqrt{\frac{1}{n}\sum_{i=1}^{n} z_i^2}$$

where n indicates the number of data, z_i the change in altitude recorded in the i-point compared to the mean height value, defined in such a way that the arithmetic sum of all the rejects is equal to zero. Specifically, Rq was calculated as the mean square root of the changes in channel z compared to the average height value calculated over the entire scanned area, previously modified with a second order digital flattening and digital bow for reduce warp and distortion effects in general three-dimensionality of the sample. To obtain a more accurate roughness values, Rq was calculated as the average value of 20 areas of 1 μm*1 μm for each acquisition carried out on the sample examined. The obtained results were analyzed and graphed using the OriginPro software (OriginLab, version 8.5, Northampton, MA, USA).

2.4.5. Tribological measurements

The friction coefficient (μ) of chitosan samples was evaluated using an NTR3 Nano Tribometer (Anton Paar GmbH, Graz, Austria) equipped with an ST-S type cantilever. The samples were loaded onto a metal support for sliding tests, and a 5-mm glass disc probe was used for this purpose. The specimens were moved at a sliding speed of 0.3 mm/s against the glass probe for a full amplitude of 1 mm. Each test was run for a total of 50 cycles with a load of $F_n = 10$ mN, and five acquisitions were performed for each sample at the acquisition frequency of 50 Hz. Coefficients of friction (CoFs) values were referred to the average value of the linear region of the central 25 cycles to avoid transient effects.

2.4.6. Thermogravimetric analysis

The thermal stability was performed using thermogravimetric analysis by TGA Q50 (TA instrument). To perform the analysis, all the samples were cut into small pieces of about 0,1x0,1 cm

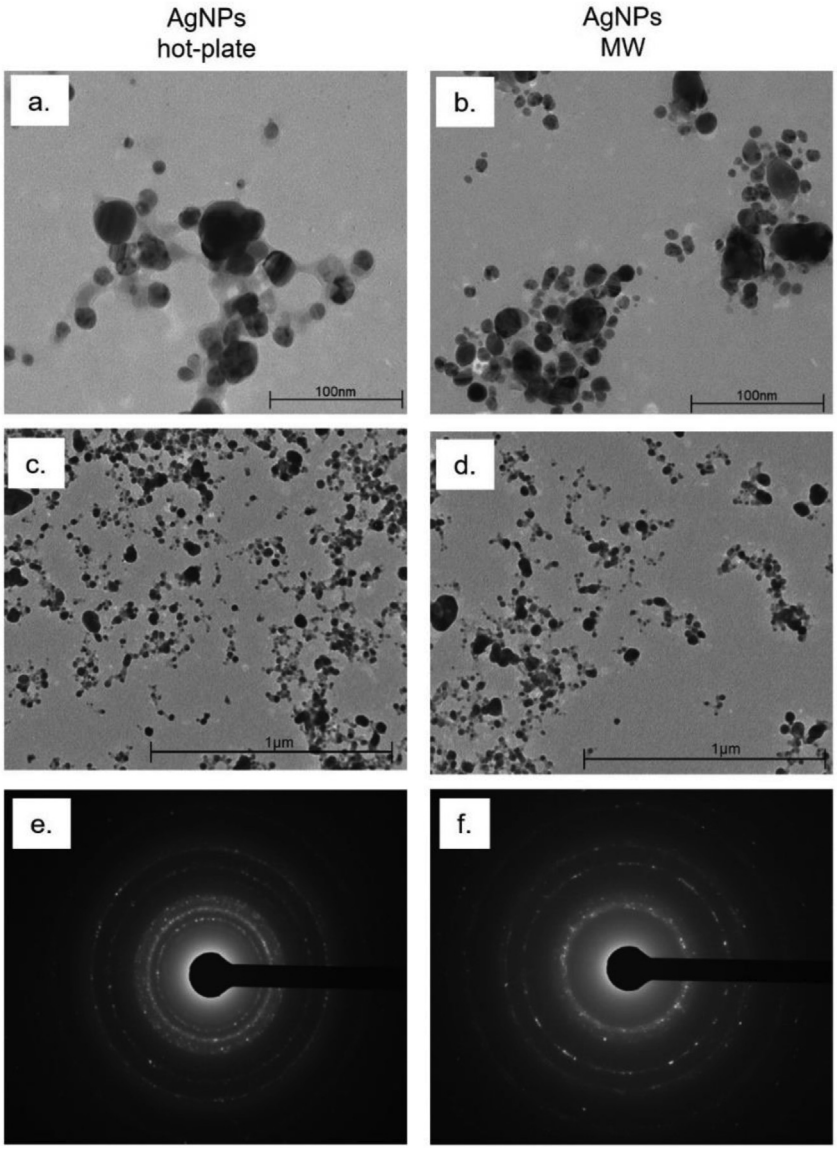

Fig. 2 – TEM acquisitions at different magnifications (100 nm and 1 μm) carried out on green AgNPs obtained by using hot-plate (a,c), and MW (b,d) synthetic routes. SAED pattern for AgNPs hot-plate (e) and AgNPs MW (f).

having a weight of 10 mg. films were heated in a temperature range of 30–600 °C with a heating rate of 10 °C/min under N_2 (30 mL/min).

2.4.7. *Ag $^+$ release study of AgNPs-chitosan composite film*

The release of Ag ions (Ag^+) from the CS/AgNPs composite films was measured at pH 5.5 and pH 6.5 for after 7 days of immersion. Briefly, each sample was immersed in water with adjusted pH using HCl at 25 °C. The released Ag^+ were quantified by ICP-OES (PerkinElmer AVIO 500).

2.5. *Toxicity studies*

2.5.1. *Cell culture*

SH-SY5Y cells were maintained in Dulbecco's Modified Eagle Medium (DMEM) (Sigma–Aldrich, Dorset, UK) with 50 μM of glutamine, supplemented with 100 U/mL of penicillin/streptomycin (Sigma–Aldrich, Dorset, UK) and 100 mg/mL of 10% Fetal Bovine Serum (FBS) (Sigma–Aldrich, Dorset, UK). The cells were incubated in a humidified controlled atmosphere with a 95%–5% ratio of air/CO_2 at 37 °C.

2.5.2. *Viability assay of SH-SY5Y*

The metabolic activity SH-SY5Y cells was measured after 24 h and 48 h, using the highly water-soluble tetrazolium salt WST-8 (Cell Counting Kit-8 Sigma Aldrich); assays were performed in 96-well microplates for each time. 0.1% of Triton X100 solution (10 μL) (Sigma–Aldrich) were added to cells as positive control. Cells were seeded in 96 well microplates at a density of 5000 cells/well and incubated for 24 h and 48 h. Following these time points, 10 μL of WST-8 solution was added to each well and the microplates were incubated for 3 h in a humidified atmosphere of 5% CO_2 and 37 °C. Subsequently, the

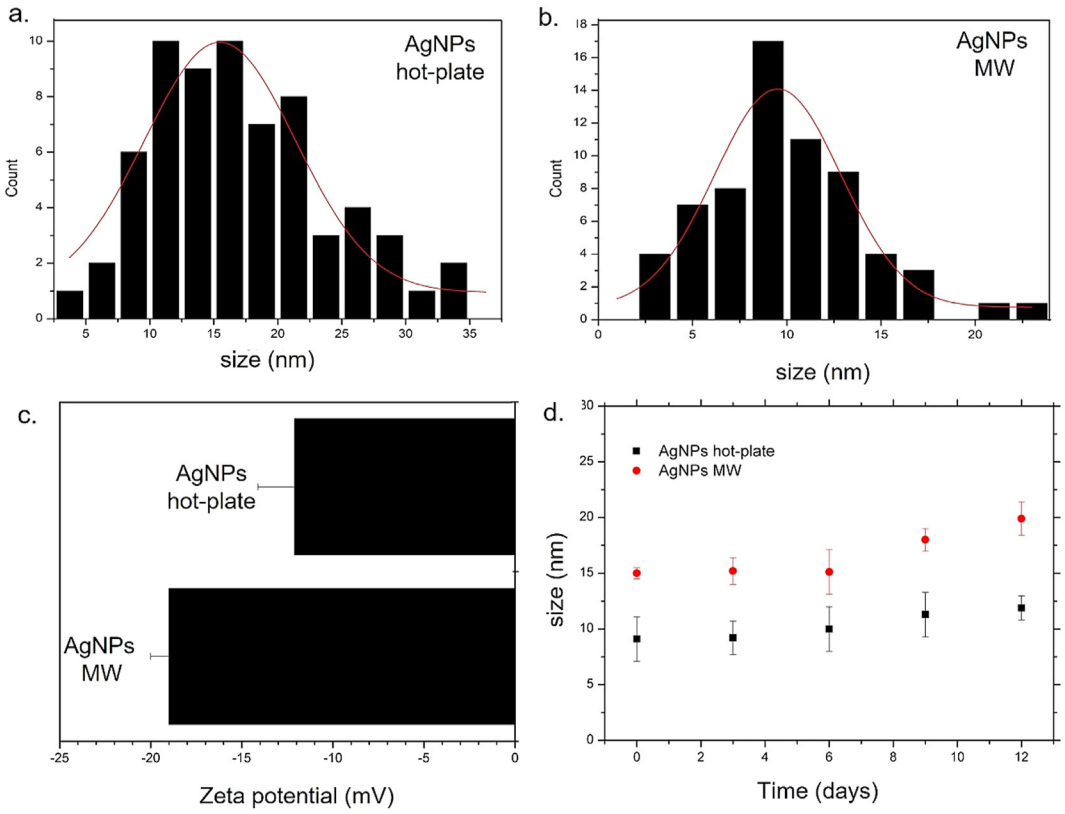

Fig. 3 – Size distribution and related statistical analysis with Gaussian fit (red line) of AgNPs achieved by hot-plate (a) and AgNPs obtained by MW routes (b). ζ-potential analysis (c) and stability studies in water (pH 7) up to 12 days.

absorbance of orange WST-8 formazan product was recorded spectrophotometrically.

2.5.3. *Cell growing on chitosan films*

The cell growth was assessed by seeding 10^3 cells on chitosan films placed in Petri dish full ofcell culture medium. After 48 h the cells images were acquired using Leica optical microscopy.

2.6. *Statistical analysis*

Statistical analyses were performed using OriginPro (version 8.1). The difference between three and more groups was analyzed through one-way or two-way ANOVA multiple comparisons, respectively. The differences between two groups were evaluated by a two-tailed Student's-test. The differences were considered statistically significant for * $p < 0.05$, ** $p < 0.01$, *** $p < 0.001$).

3. Results and discussion

Nowadays, the reduction of toxic substances in some kinds of industrial and commercial products is a critical issue [29]. In this aim, the principles of green chemistry have the final goal to produce safe materials through less impactful processes [30]. Therefore, the nanostructured materials obtained by eco-friendly routes match with green chemistry principles, since it involves the use of vegetable substances or microorganism extracts as chemical reagents. *Aloe Vera* is a succulent plant belonging to the family of the Asphodelaceae, which grows in tropical climates and its cultivation is done for medical and cosmetic purposes [31]. The *Aloe Vera* leaves contains gel having known therapeutic properties. This gel is enclosed and protected by epidermic layers, which represents the 30% of the total weight. The leaves are waste products, that are disposed after gel extraction.

In the present study, the proposed green synthetic path consisted in the replacement of sodium citrate ($Na_3C_6H_5O_7$) and sodium borohydride ($NaHB_4$), commonly employed in conventional syntheses, with foliar extract of *Aloe Vera*, rich of biomolecules acting both as reducing and capping agents in the presence of $AgNO_3$. The extract was used to carried out: (i) synthesis with specific temperature provided by the hot-plate and (ii) synthesis by microwaves (MW) as described in materials and method section. The isolated NPs obtained by hot-plate approach were analyzed by TEM, resulting almost spherical (Fig. 2 a, c). Furthermore, it was possible to notice some structures having different contrast enveloping the NPs, most likely due to the presence of organic residues normally present in the leaf extract. The average size value was (15.5 ± 0.7) nm.

To optimize the synthetic protocol, i.e. decreasing of working time, energy consumption and reagent volumes, we moved to achieve AgNPs by a procedure requiring a domestic microwave oven, starting from leaf extract of *Aloe Vera* and $AgNO_3$. Microwaves oven works at a MW frequency of

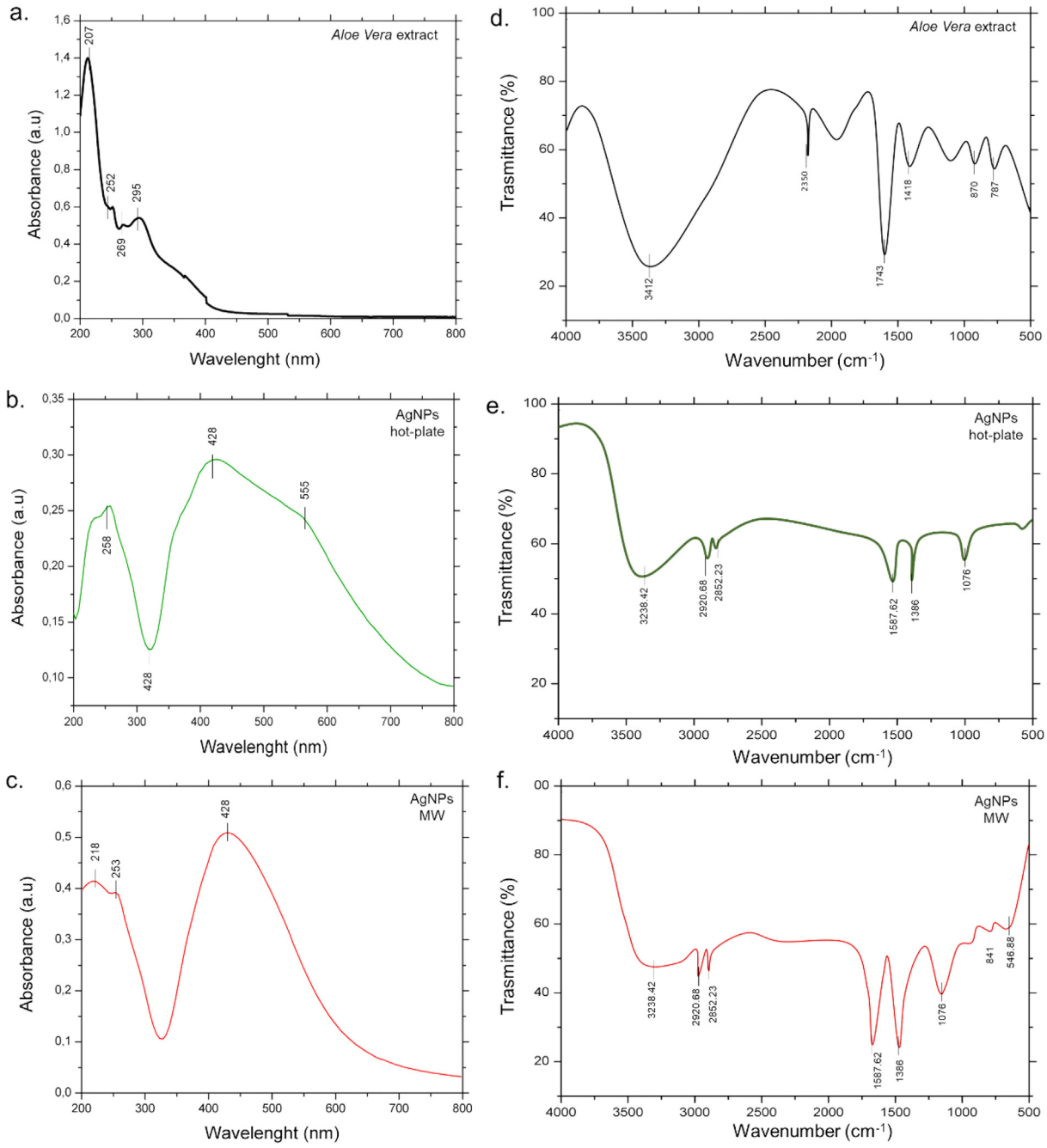

Fig. 4 – UV–vis and FTIR measurements acquired on *Aloe Vera* extract (a,d), on AgNPs obtained by hot-plate (b,e) and microwaves respectively (c,f).

oscillation frequencies equal to 2.45 GHz generating heating that uniformly spread in the solution. Preliminary tests were performed to determine MW power and reaction time, maintaining constant the volume of solution and leaf extract. The obtained results shown that the optimal parameters to achieve AgNPs were 385 W of MW power for 300 s, starting from 1 mM $AgNO_3$ aqueous solution mixed with leaves extract. Also in this case, the MW-obtained AgNPs were characterized by TEM (Fig. 2 b, d). NPs had a diameter of (9.5 ± 0.4) nm, lower than NPs obtained by hot-plate-based protocol; the shape of the AgNPs remained hemispherical; again, the NPs surfaces appeared covered by residues of organic material. SAED (Selected Area Electron Diffraction) acquisitions, performed on AgNPs obtained by the two different synthetic methods, shown the presence of typical concentric rings indicating that the NPs were crystalline and with a random orientation in both type of green NPs.

Size distribution of NPs were performed selecting 70 nano-objects for each type of NP on TEM acquisitions using ImageJ software. Data were statistically analyzed by Gaussian fit (Fig. 3 a. b). The measure of ζ-potential on NPs permits to have information about their stability. Generally, high value of ζ-potential indicates a greater stability of the colloidal solution as the electrostatic repulsion acting between the dispersive

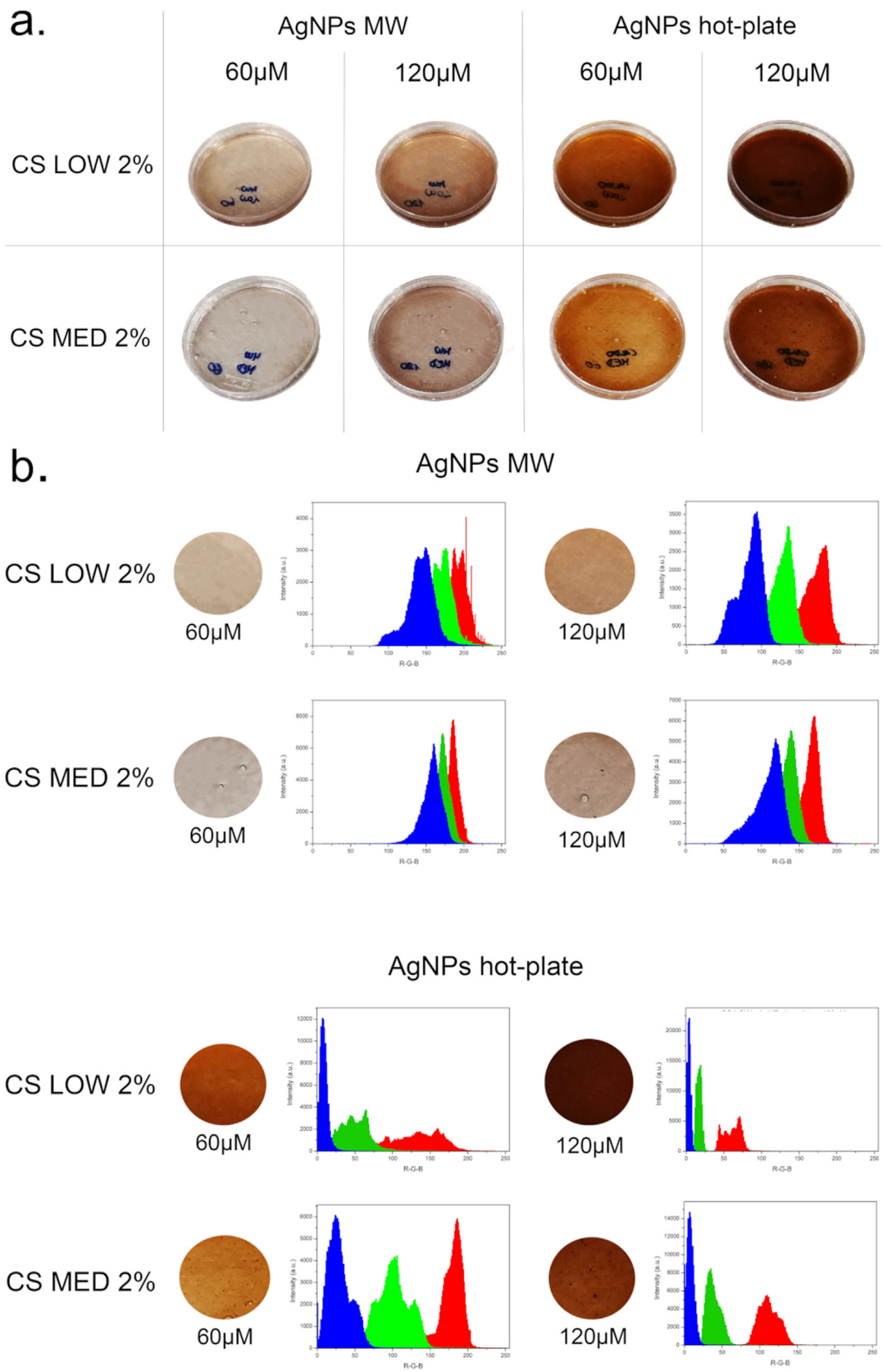

Fig. 5 – CS (low and medium) films with AgNPs achieved by hot plate and MW routes. The CS films were obtained by drop casting in *petri* dishes at different concentrations (a) and relative RGB analysis (b). Images were acquired by mean a commercial photocamera.

medium and the NPs prevents aggregation. The AgNPs from hot-plate route shown value of (−12 ± 3) mV, whereas for AgNPs produced by MW, the value was (−19 ± 3) mV (Fig. 3 c). The negative charge, due to the presence of organic capping agents containing many−OH groups, is an ideal condition for the subsequent addition in CS, it has protonated amino groups in aqueous solution. The higher zeta potential value of AgNPs from MW indicated greater colloidal stability as well as greater interaction with the CS compared to the AgNPs produced with hot-plate. We then assessed the stability of the two types of AgNPs at 3, 6, 9, and 12 days by DLS (Fig. 3d). As expected, the size did not change up to the 6th day; after this time point, some aggregation phenomena were observed, probably due to the organic shell onto NPs.

UV−vis absorption spectroscopy allowed to confirm the formation of AgNPs analyzing a range of wavelengths between 200 and 800 nm. Generally, Surface Plasmon Resonance (SPR) for colloidal solutions of AgNPs generates an absorption in the range of (400−450) nm. UV−vis spectra of the two types of AgNPs were reported in (Fig. 4 b,c), as well as the relative spectra of *Aloe Vera* plant extract (Fig. 4a). In the latter, the peak at 295 nm was associated organic compounds such as polyphenols and carbohydrates; in addition, peaks at 253 nm and 269 nm were indicative of the anthraquinones presence [32]. The absorption curve of Fig. 4b was relative to AgNPs obtained by hot-plate route. As displayed in the graph, two peaks related to the plant extract were reported; the peak at 420 nm was specific of AgNPs plasmon peak. In addition, it was visible a small peak, at 550 nm, attributable to longitudinal and transversal plasmon resonance of AgNPs [33]. The UV−vis measurement of AgNPs obtained by MW showed similar spectra. The peak at 428 nm was specific of AgNPs whereas the blue-shift peaks were related to organic molecules (Fig. 4c).

Following that, FTIR spectroscopy investigation was conducted to study infrared absorption of the AgNPs and to analyze the chemical groups. For this purpose, the FTIR spectra of the AgNPs solutions were compared with those of the plant extracts achieved in the same experimental conditions, used to synthesize AgNPs. The *Aloe Vera* extracts exhibited a broad absorption band centered at 3412 cm^{-1}, due to the stretching of −OH groups, a characteristic of carbohydrate monomers including mannose and uronic acid (Fig. 4d). The absorption band at 1743 cm^{-1} indicated the presence of carbonyl groups of *Aloe Vera*, whereas 1418 cm^{-1} peak was associated with the asymmetrical and symmetrical −COO stretching of carboxylate compounds in *Aloe Vera*. The absorption peak at 870 cm^{-1} was due to the C−H out ofplane deformation of carbohydrate monomers. In Fig. 4e and f were reported the spectra related to AgNPs derived from hot-plate and MW respectively. In particular, the peak at 3238.42 cm^{-1} was associated to OH groups whereas, the peaks at 1587.6 cm^{-1} (C=C groups or from aromatic rings), 1386.4 cm^{-1} (geminal methyl), and 1076 cm^{-1} (ether linkages) suggested the presence of flavanones or terpenoids on the surface of synthesized AgNPs.

Following the physical characterization of AgNPs, they were added in CS solutions (low and medium molecular weight, 2%) to obtain two final concentrations of 60 μM and 120 μM. The images of the films deposited in the *petri* dishes after polymerization were reported in Fig. 5a.

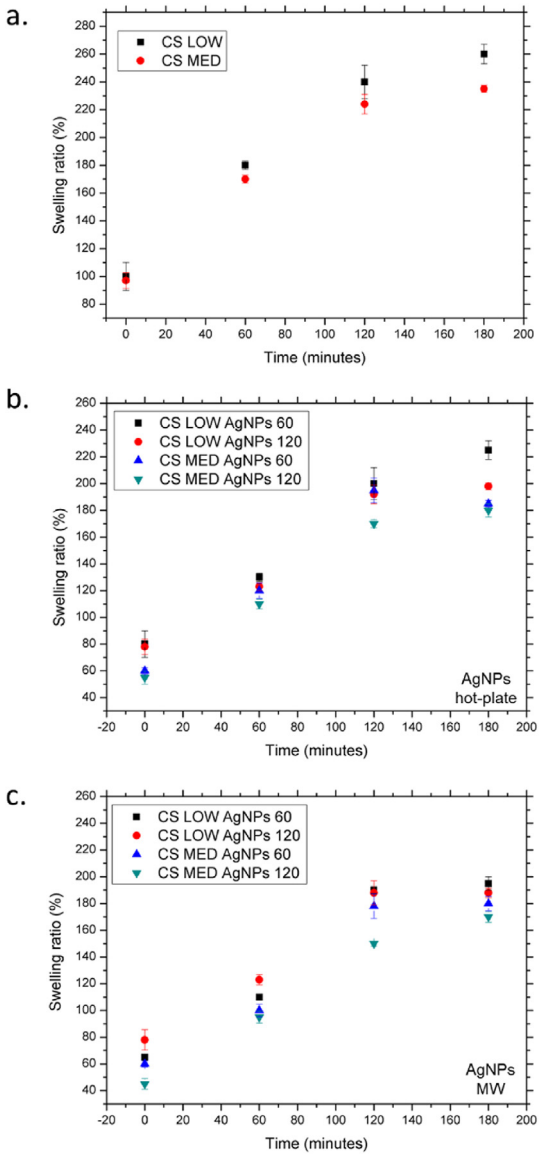

Fig. 6 − Swelling ratio expressed as percentage of nanocomposite films with AgNPs at concentration of 60 and 120 uM. The samples were prepared using AgNPs from hot-plate and microwaves syntheses as described in the section materials. The experiments were conducted in MilliQ water at temperature of 25 °C and pH 6.8.

The chromatic analysis of images was performed using ImageJ software through the evaluation of the RGB channels in the central region of each sample. The samples were placed on a white background to evaluate their transparency; the images were acquired under the same lighting conditions and through the same commercial camera. The data reported in Fig. 5b showed the different red, green and blue components quantified by a scale in the range of 0−255; the three components at the minimum of the scale indicated a black color; on the other hand, the resulting color will be white.

The CS samples added with AgNPs achieved by MW exhibited transparent features as the RGB components fall in the high region of the scale (>100) and were almost entirely

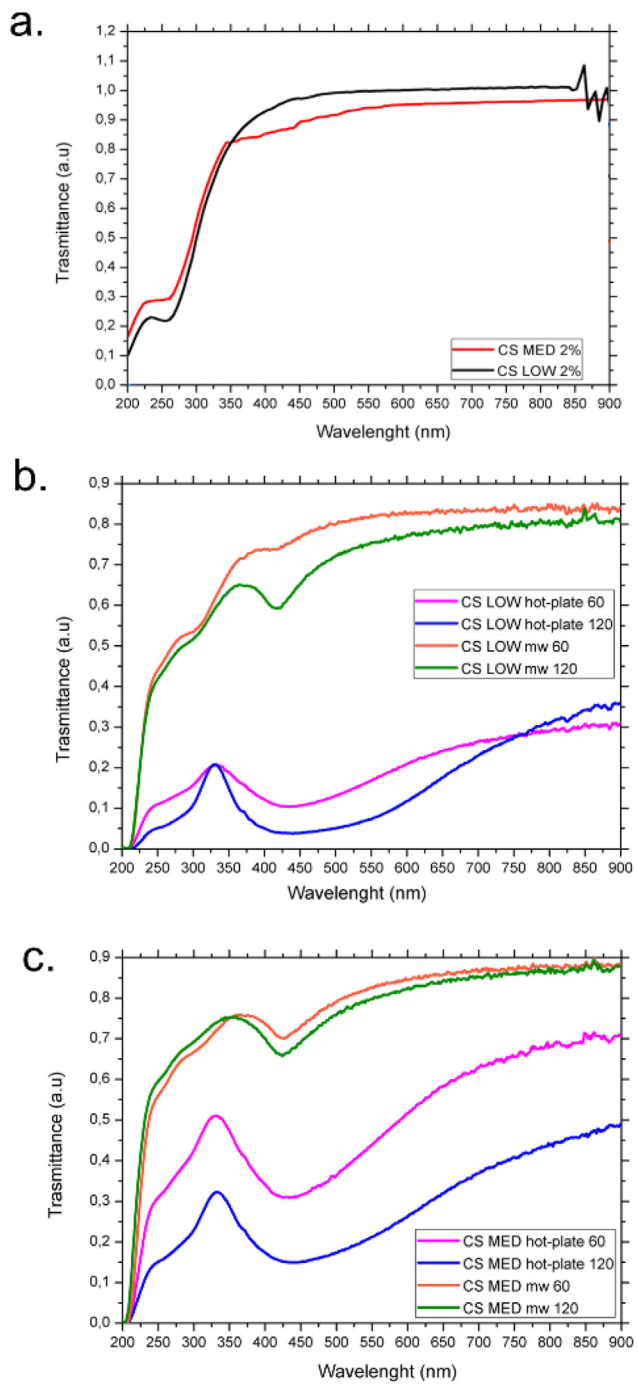

Fig. 7 – Transmittance spectra of low and medium CS control films (a), chitosan films low (b) and medium (c) with hot AgNPs -derived from hot-plate and MW at two concentrations, i.e. 60 μM and 120 μM.

superimposed, indicating a white of the reference background. The samples added with AgNPs derived from hot-plate instead have a darker color and the chromatic components were shifted to lower values. In the last case, the dominant component was the red one.

After polymerization, the films enriched with AgNPs were analyzed by several techniques in order to evaluate their suitability for food packaging applications. To this aim, the swelling ability represents a critical parameter [34]. In the CS-based film, the swelling activity is strongly dependent by the CS chains interactions and consequently by the cross-linking density [35]: in general, when the density is high, the swelling capacity is low [36]. Furthermore, CS has a positive charge that permits to retain a great amount of water in its chains; sure enough, it has been proven the CS ability to absorb water in wet environments due to its hydrophilic properties [37]. Considering these evidence, each sample (control samples, namely CS low and medium without NPs and films with Ag NPs) was immersed in water in order to understand the swelling capacity. Successively, the films weight was monitored at different time points, i. e 0, 60, 120 and 180 min (Fig. 6).

The water absorption resulted time dependent from 0 to 120 min both for controls and samples with AgNPs. In particular, the pure CS showed a high swelling degree, which increased from 100 (t = 0) to ~260% for low CS and to ~235% for medium CS after 180 min (Fig. 6a). Thus, it was evident that the low molecular weight was more susceptible to the water absorption than medium CS. This was true because the higher molecular weight polymers exposed less chain ends, corresponding to a less free volume. This phenomenon increased the density of the CS, making the medium CS less able to attract water [38]. When AgNPs were added in the CS solution, the swelling ratio diminished. This phenomenon can be explained by the capacity of Ag^{+} to cross-link CS chains due to the bind between ammine and hydroxylic groups of CS and AgNPs respectively. Thus, this bond reduced the penetration of water molecules into the films, decreasing the swelling ability [39]. For nanocomposite samples, it was evident that the swelling ratio of films was influenced by NPs concentrations and size. As showed in Fig. 6b, the AgNPs (120 μM) derived from hot-plate reduced the swelling ability whereas the concentration of 60 μM reached values comparable to control samples after 180 min of experimental time. However, the low CS adding 60 μM of AgNPs exhibited the higher swelling ratio respect to the same films developed using medium CS after 180 min (223% versus 195%). The swelling ratio of CS-based films was strongly influenced when the AgNPs size was reduced. As shown in Fig. 6c, the swelling % values were reduced when the AgNPs obtained from MW were added in the CS solution. Also in this case, this effect was clearer using CS medium weight. This result can be explained with a better dispersion of the MW-achieved AgNPs in the polymeric solution [40].

The optical behavior of CS films was investigated by transmittance measurements (Fig. 7). The optical properties of polymers suitable for wrapping and preserving foods are critical, as these films should be able to screen out light, and in particular its UV component, which could alter the food quality. The CS is sensitive to light because its chains can undergo degradation; so, the optical properties of CS films are measured in terms of transmittance. In general, the mostly commercially plastics are transparent because the addition of dyes is not feasible due to their poor solubility in the polymer matrix [41]. Then, we proceed to analyze the transmittance behavior of our nanocomposite films compared values with control samples (Fig. 7). As expected, the control samples were almost transparent: the transmittance values acquired in the wavelength range of 250–900 nm were 0.98 and 0.92 for low and medium CS, respectively. The addition of the two types of green AgNPs

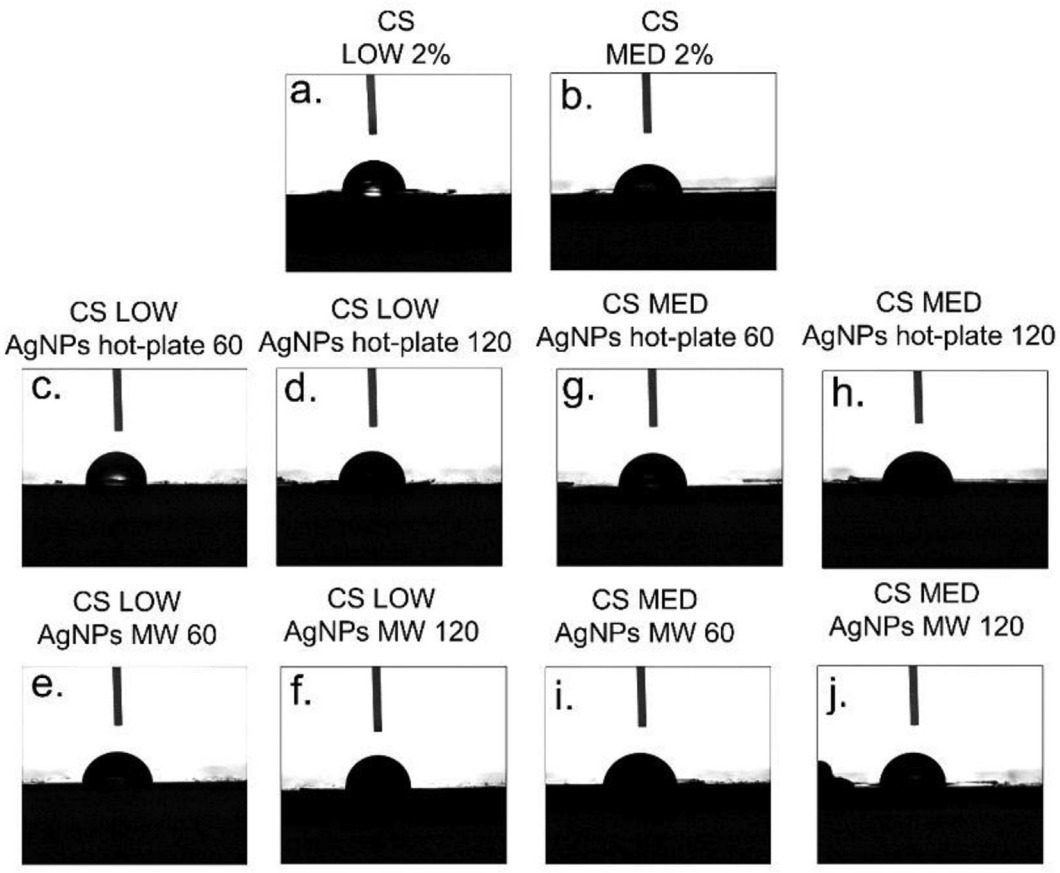

Fig. 8 – Water drop profile at t = 0 on control CS films (low and medium chitosan 2%) and CS films with AgNPs obtained by two different routes at two concentrations (60 μM and 120 μM).

reduced the transmittance values (Fig. 7b and c); this effect become more pronounced in low CS film enriched with AgNPs synthetized using the hot-plate based protocol. These experimental findings appeared in accordance with the color change of CS films due to different NPs addition as previously shown. Indeed, the films prepared with 120 μM of NPs, in visible and near infrared regions exhibited transmittance values lowered to 0.28 (28%) for low CS films prepared with hot-plate synthesized AgNPs, whereas the values reached 0.48 (48%) for the correspondent addition in medium CS. On the other hand, the transmittance measurements related to nanocomposite films with AgNPs achieved by hot-plate reached about 0.85 (85%) for both low and medium CS. Contrary, the transmittance related to the samples formed by AgNPs MW, displayed optimal behavior reaching good values both for low and medium CS. As showed in Fig. 7b and **c**, the transmittance reaching maximum value of 0,72 (72%) for low CS films with the addition of AgNPs MW (60 μM and 0,75 (75%) for the two concentrations of AgNPs in medium CS. Then, the films with AgNPs derived from MW synthesis were more transparent respect to the same with AgNPs from hot-plate. Absorption peaks in the range of 400–450 nm indicated the plasmonic absorption of NPs.

Table 1 – Contact angle θ values measured at t = 0 s, t = 1 s and t = 3 s of CS low and medium 2% films (control samples) and on CS films with AgNPs obtained by two different routes at two concentrations (60 μM and 120 μM). Results were statistically significant performing an ANOVA test for *p* value < 0.05.

AgNPs hot plate			
Samples	$\theta t = 0(^\circ)$	$\theta t = 1(^\circ)$	$\theta t = 2(^\circ)$
CHITOSAN LOW 2%	78 ± 1	77 ± 1	77 ± 1
CHITOSAN LOW AgNPs 60	85 ± 2	85 ± 3	84 ± 2
CHITOSAN LOW AgNPs 120	79 ± 3	79 ± 2	79 ± 3
CHITOSAN MED 2%	77 ± 1	76 ± 2	76 ± 1
CHITOSAN MED AgNPs 60	83 ± 2	83 ± 2	82 ± 1
CHITOSAN MED AgNPs 120	78 ± 2	77 ± 2	77 ± 1
AgNPs MW			
Samples	$\theta t = 0(^\circ)$	$\theta t = 1(^\circ)$	$\theta t = 2(^\circ)$
CHITOSAN LOW 2%	78 ± 1	77 ± 1	77 ± 1
CHITOSAN LOW AgNPs 60	84 ± 3	81 ± 3	81 ± 3
CHITOSAN LOW AgNPs 120	88 ± 1	88 ± 1	88 ± 1
CHITOSAN MED 2%	77 ± 1	76 ± 2	76 ± 1
CHITOSAN MED AgNPs 60	77 ± 1	77.3 ± 0.1	77.0 ± 0.2
CHITOSAN MED AgNPs 120	83 ± 2	82 ± 2	82 ± 1

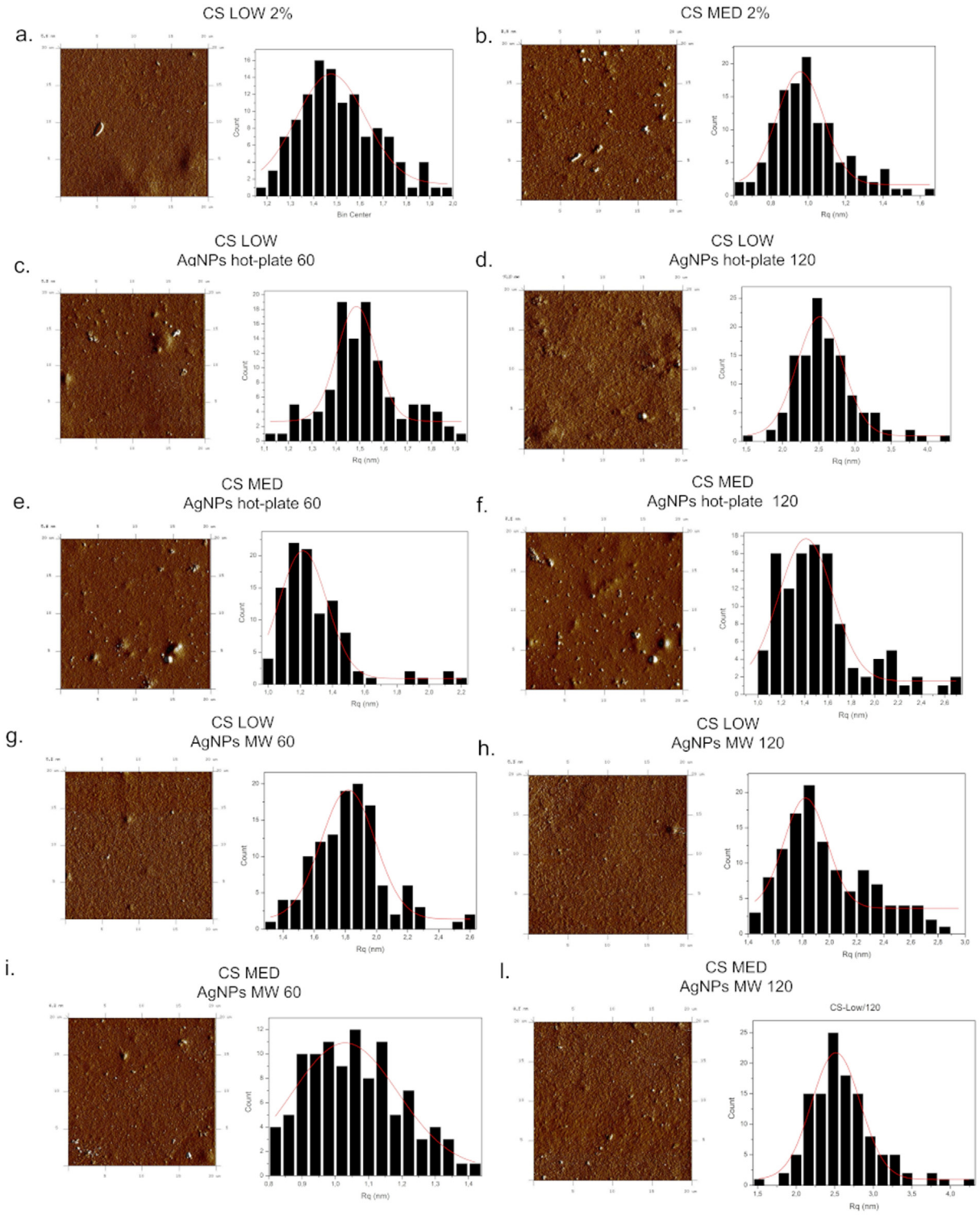

Fig. 9 – Representative AFM acquisitions for low and medium CS control samples (a,b) and nanocomposite films with AgNPs from hot-plate (c-f) and microwaves at 60 μM and 120 μM (g-l). AFM Images were reported in the 3D merge channel which overlaps the measurement of the channel's height and deflection error. The histograms correlated to the AFM acquisitions reported the roughness analysis and the Gaussian fit (red line) used to extract the Rq mean value and associated standard deviation on the different CS low and medium molecular weight films without and with AgNPs. The measurements were statistically significant by performing an ANOVA test for a p value < 0.05.

Table 2 – Roughness (Rq) values obtained from the analysis of 120 1 μm*1 μm areas per sample, related to six different topographic analyses per film and comparation with contact angle values.

Samples	Rq (nm)	$\theta t = 0(^{\circ})$
CS LOW 2%	1.4 ± 0.01	78 ± 1
CS LOW hot-plate AgNPs 60	1.5 ± 0.01	85 ± 1
CS LOW hot-plate AgNPs 120	2.5 ± 0.02	79 ± 3
CS LOW MW AgNPs 60	1.8 ± 0.02	84 ± 3
CS LOW MW AgNPs 120	1.9 ± 0.02	88 ± 1
CS MED 2%	1.0 ± 0.01	77 ± 1
CS MED hot-plate AgNPs 60	1.2 ± 0.01	83 ± 3
CS MED hot-plate AgNPs 120	1.4 ± 0.03	78 ± 1
CS MED MW AgNPs 60	1.1 ± 0.02	77 ± 1
CS MED MW AgNPs 120	1.5 ± 0.03	83 ± 2

With the aim to understand if these films were suitable for food packaging, the film wettability is another important parameter to consider. In general, the hydrophilic nature of CS could be an obstacle in CS application because they can be damaged by water inducing collateral effects, as microorganisms and moulds proliferation. Then, wettability studies were performing measuring the contact angle formed between a water drop and the film surface [42]. when the contact angle (θ) increases, the interaction of the two elements decreases [43]. Based on θ value, it is possible to determine whether a surface has a hydrophilic or hydrophobic nature when in contact with water; in the latter circumstance, the film will be characterized by good wettability [44]. The data reported in the literature describe CS as a hydrophobic material, with a contact angle value ranging from about 75° to about 90°, depending on the molecular weight and the degree of deacetylation (DA) [44–46]. In addition, the use of nanofillers in the polymer matrix is expected to bring an improvement in the properties of the CS [47]. Five drops were deposited on the CS low and medium molecular weight as controls (Fig. 8 a, b) and CS films with AgNPs (60 μM and 120 μM) from hot plate (Fig. 8 c, d, g, h) and microwaves routes (Fig. 8 e, f, I, j). The contact angle measurements were carried out at three different times, t = 0 s, t = 1 s and t = 2 s, in order to evaluate the stability in the first instants after droplet deposition. The data were tabulated in Table 1.

As reported, θ remained nearly stable in the first moments of droplet deposition, indicating good stability of the film.

Table 3 – Friction coefficients (CoF) of CS low and medium (control samples) and CS with addition of AgNPs obtained by using hot-plate and MW -based protocol.

Samples	Friction coefficient (CoF)
CS LOW 2%	0.130 ± 0.002
CS LOW hot-plate AgNPs 60	0.127 ± 0.001
CS LOW hot-plate AgNPs 120	0.107 ± 0.001
CS LOW MW AgNPs 60	0.140 ± 0.001
CS LOW MW AgNPs 120	0.120 ± 0.002
CS MED 2%	0.12 ± 0.001
CS MED hot-plate AgNPs 60	0.090 ± 0.003
CS MED hot-plate AgNPs 120	0.100 ± 0.001
CS MED MW AgNPs 60	0.100 ± 0.002
CS MED MW AgNPs 120	0.150 ± 0.001

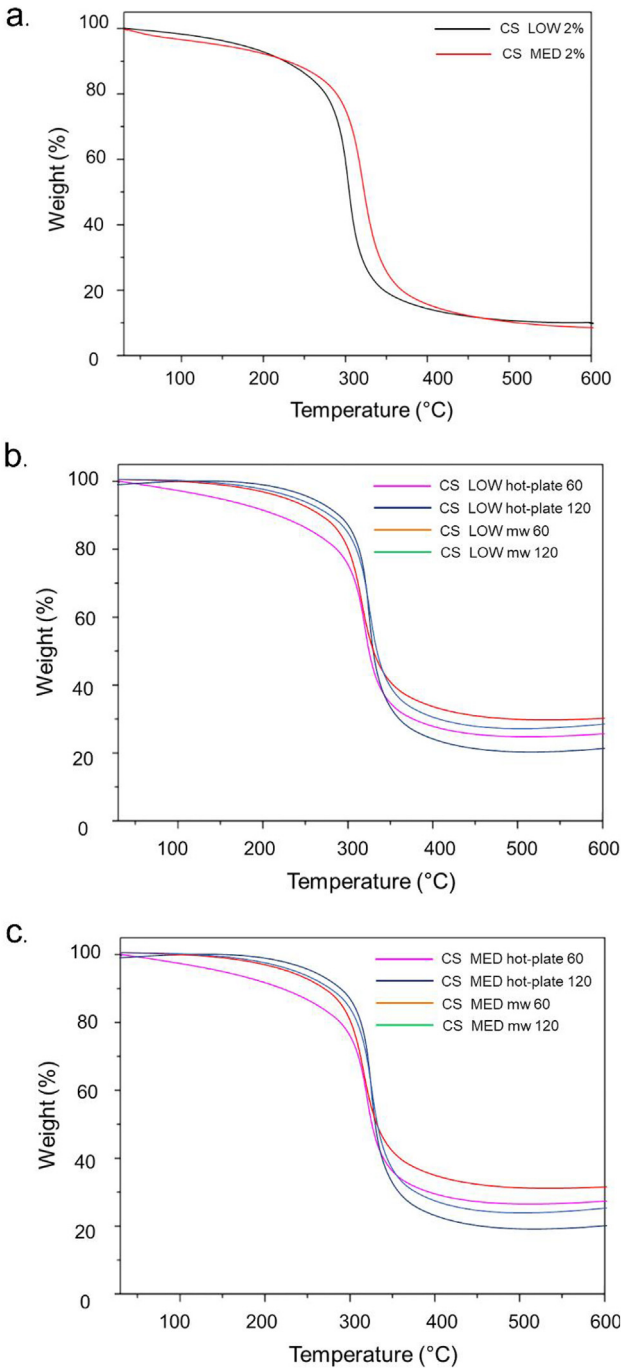

Fig. 10 – Thermal stability analysis of low and medium CS control films (a), chitosan films low (b) and medium (c) with AgNPs derived from hot-plate and MW routes at two concentrations, i.e. 60 μM and 120 μM.

Despite differing in molecular weight, the control samples, i. e low and medium CS without NPs, exhibited a comparable θ, that was (78 ± 1) for low and (77 ± 1) for medium CS.

The addition of AgNPs as nanofillers in the CS matrix induced a wettability improvement in all cases. Specifically, the θ value f was dependent on the NPs concentration: films of CS formed by the addition of NPs obtained using hot-plate synthesis an θ increase was observed using 60 μM of AgNPs

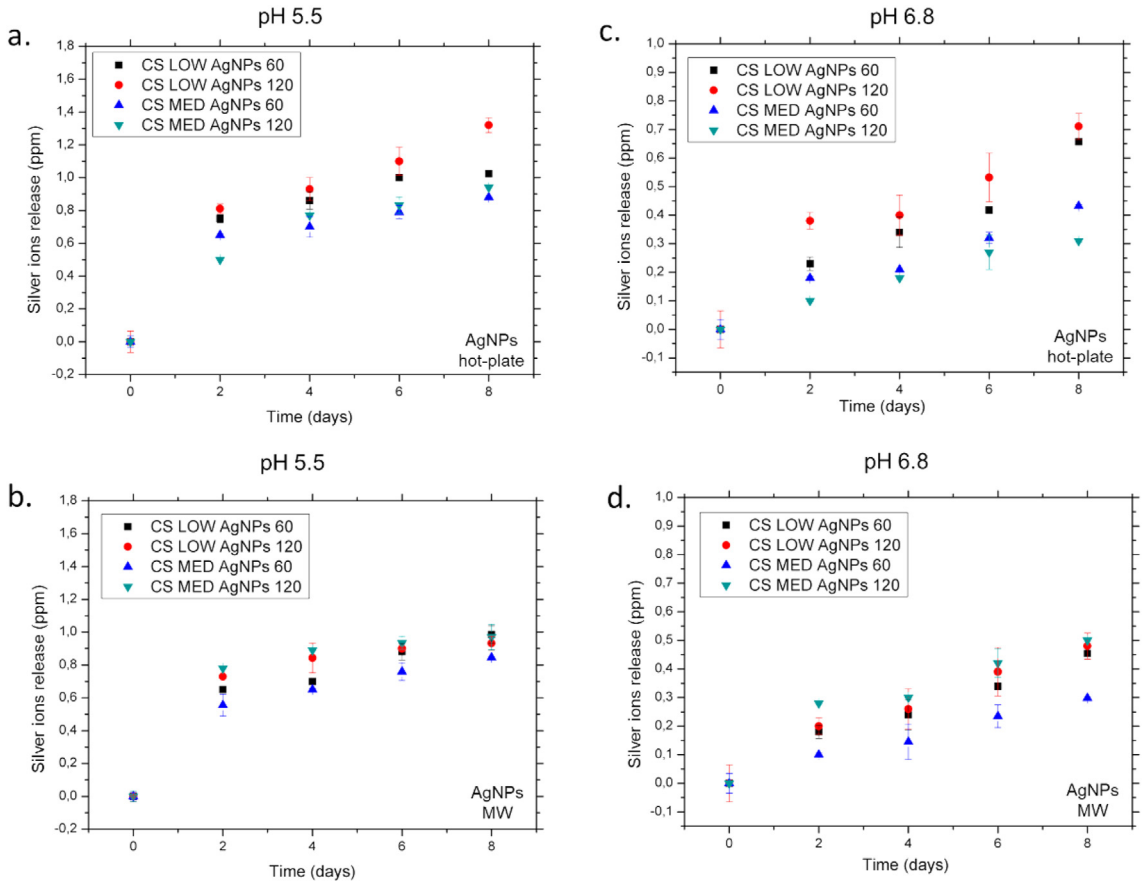

Fig. 11 – Release of Ag^+ from the CS low AgNPs and medium CS AgNPs at concentration of 60 and 120 μM at pH 5.5 (a,b) and pH 6.8 (c,d). The samples were prepared using AgNPs from hot-plate and MW syntheses as described in the section materials.

and a subsequent decrease when the NPs concentration of 120 μM was apply. In detail, using the low CS with 60 μM and 120 μM of AgNPs derived from hot-plate the values were (85 ± 2) and (79 ± 3) respectively. Similar data were recorded using medium CS (Table 1).

In contrast, AgNPs synthesized by MW conferred a wettability improvement, observable by θ increase when concentration of NPs grown. This different behavior between the two types of samples can be associated to the synthetic approach employed to obtain the AgNPs and, in addition, to the different size of AgNPs, resulting larger for those synthesized with hot-plate. Indeed, the size of the NPs and polymer chains, which are comparable, implies that the diffusion processes of the NPs compete with those of the polymer chains, which can therefore lose their structural regularity, inducing a change in the film properties [48].

Moreover, the smaller size of AgNPs also resulted in a higher value of surface area/volume ratio, which implied a larger area at the interface with the polymer chains. Also, the higher surface charge of AgNPs obtained by MW conferred a more chemically stable bonding between the nanostructures and the CS chains.

The samples of low CS produced using AgNPs from MW exhibited the highest value of θ and greater stability in the first moments of contact with the water droplet (84 ± 3) for 60 μM and (88 ± 1) for 120 μM; this result suggested that these films can be suitable for food packaging applications, supported by the transparency properties. However, the transmittance studies, suggested that the AgNPs obtained by hot-plate conferred a darker coloration to the films protecting from visible and near infrared light.

To correlate wettability with roughness, the surface area of each nanocomposite films was examined by Atomic Force microscopy (AFM) measurements at high resolution (Fig. 9). We reported the AFM acquisitions of control samples in Fig. 9 a, b and the relative average Rq values. The AFM images of low and medium CS prepared with hot-plate derived AgNPs (60 μM and 120 μM) and their Rq were listed in Fig. 9 c, d, e, f. Similarly, Fig. 9 g, h, i, l referred to AFM scans performed on low and medium CS enriched with AgNPs from MW with the correspondent Rq.

The Rq values were reported in Table 2.

In general, it was evident that the AgNPs addition in CS matrix induced an increase of Rq parameter in concentration dependent manner respect to the correspondent control sample. Specifically, the addition of AgNPs (60 μM) derived from hot-plate route in low CS induced a growth of the Rq value to ~7% whereas the increment reached the 79% in the case of high concentration of AgNPs in CS. Same trend was recorded in medium CS, in which the Rq increased of 20% and

Table 4 – Ag^+ values (expressed in ppm) from nanocomposite films measured in the experiments reported in Fig. 11 after 8 days at acidic conditions (pH 5.5).

samples	CS LOW Hot-plate AgNPs 60	CS LOW hot-plate AgNPs 120	CS MED hot-plate AgNPs 60	CS MED hot-plate AgNPs 120	CS LOW MW AgNPs 60	CS LOW MW AgNPs 120	CS MED MW AgNPs 60	CS MED MW AgNPs 120
ppm (Ag^+)	1.02	1.32	0.88	0.94	0.98	0.93	0.85	0.97

40%, respectively. Similarly, the addition of AgNPs from MW caused a raise of Rq values depending on NPs dosage; indeed, the rate was equal to ~29% and ~36% following the addition of 60 μM and 120 μM of AgNPs in low CS respectively; in medium CS the percentages was ~10% and 50%, respectively.

Comparing the values of Rq with the contact angle data, it was interesting to observe some contrast behaviors when correlate low and medium CS and the different AgNPs. As shown in Table 2, when Rq increased according to the concentration of hot-plate-derived NPs, the contact angle values decreased. Contrary, the addition of AgNPs achieved by MW, determined the growth both in Rq and contact angle values. These experimental findings might help to understand the thermodynamics behavior of nanocomposite films in contact with a liquid droplet. After incorporation of AgNPs, the hydrophobic performance of the films was significantly improved, increasing the probability of a superhydrophobic state as demonstrated in the work of Pinto et al. [49]. Since AFM analysis showed that the incorporation of NPs would drastically affect surface roughness, a rougher surface structure was one of the key factors in achieving a more hydrophobic behavior; this can be explained by the "lotus effect," whereby lotus leaves repel water due to the presence of small micro- and nano-sized protuberances on the surface. In particular, the NPs obtained by MW method added to the CS, showed a significant enhancement in terms of contact angle and Rq increase and then hydrophobicity. The difference observed with NPs obtained by hot-plate could find justification in a better dispersion in the CS matrix and to a higher colloidal stability, which improved and increased the surface hydrophobicity. As matter of fact, since the best dispersion was obtained using low CS having low viscosity, this allow to achieve an optimal contact angle value, most likely, increasing the concentration of NPs, a better performance could be obtained in terms of hydrophobicity.

Since tribological behavior is conditioned by the surface microstructure [50], which can be expressed in term of Rq, we have quantified the static friction coefficient (μ_s) by analyzing CS-based films by means nanotribometer. As showed in Table 3, no statistical differences were recorded measuring the CS films both controls and nanocomposites. This result was promising in order to develop alternative plastic materials; indeed the commonly used plastics such as PET, PLA [51], PE and PP [52] showed CoF values higher that those measured on CS films.

Furthermore, the absence of a significant change in friction coefficient value respect to the undoped CS films, suggesting that the AgNPs addition did not make the CS films prone to the crack formation or other structural damage, as well as deformation of material [50].

To understand the effect of AgNPs addition in CS films on thermal stability, thermogravimetric analysis was performed using a temperature range between 30 °C and 600 °C (Fig. 10). As previous reported, control samples were represented by polymerized low and medium CS.

Three different steps were observed in the control samples (Fig. 10 a). A first weight decrease was observed at 50–140 °C that can be associated to the water content loss. The second weight reduction appeared at 230 °C, that can be associated to the loss of water molecules strongly linked in the inner space

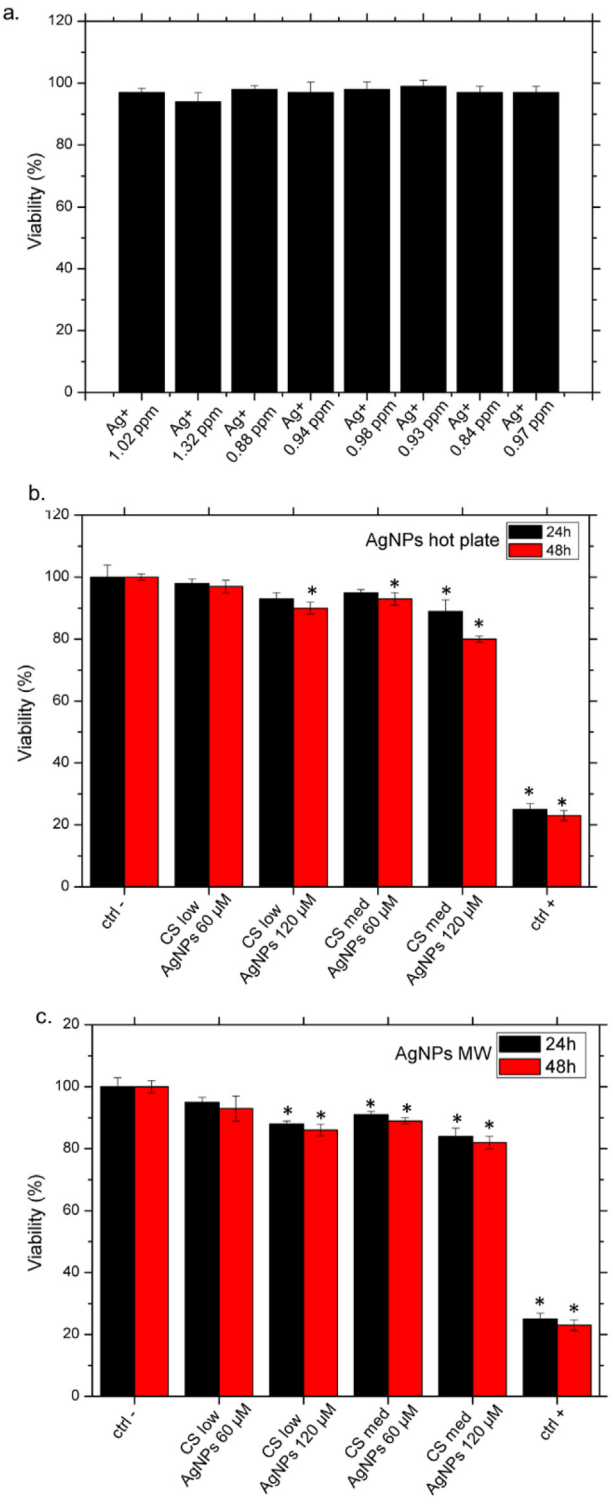

Fig. 12 – Viability assay of SH-SY5Y incubated with Ag^+ at different concentrations for 48 h. (a) Viability assay of SH-SY5Y cell lines in contact with nanocomposite films (low and med CS) formed by AgNPs from hot-plate (b) and from MW (c) evaluated at 24 and 48 h after seeding. The viability of cells growth on CS-NPs films was normalized to non-treated control cells. As a positive control (P), the cells were incubated with 5% DMSO. Data reported as the mean ± SD from three independent experiments are considered statistically significant, compared with the control ($n = 8$) for *p*value < 0.05 (<0.05 *).

of CS units. At the higher temperatures, c. a 330 °C, a depolymerization and dehydration of different carbohydrate molecules as well as the degradation of chitosan acetylated and deacetylated units were observed [53,54]. This behavior was similar for low and medium CS resulting in a weight loss of about 80%.

When AgNPs were added in the CS (Fig. 10 b,c), the thermal resistance of the films increased both for low and medium CS due to the interaction of metallic NPs with polymer chains. This effect was more evident at high temperatures. Indeed, the intramolecular connection between the components influenced the thermal properties, depending on the chemical bonds such as van der Waals forces, hydrogen bonding, hydrogen bonds and others. As observed in Fig. 10 b, at low temperatures, the spectra profile was similar to the controls, whereas when temperature increased, an improvement in thermal stability was observed, particular evident for low CS with AgNPs from MW. Same spectra were noticed in Fig. 10c, where results for medium CS was graphed.

With the idea to obtain safe films for consumers but toxic for microorganisms and moulds, we analyzed the silver ions (Ag^+) release in terms of ppm using two buffers having different pH (5.5 and 6.8), immersing all the samples prepared for the experiments previously reported.

Then, we used as control samples CS low and med 2% and the films with AgNPs achieved from hot-plate and MW at the two different concentrations (i.e 60 μM and 120 μM) (Fig. 11). As observed, the general trend showed a time and dose dependent Ag^+ release rate influenced by medium pH during 8 days. This behavior can be described by the swelling properties of CS films and, in addition, by AgNPs oxidation exerted by dissolved oxygen in water [55].

Using acidic buffer pH (5.5) (Fig. 11 a, b) it was possible to observe a higher ions release profile compared to the neutral pH (6.8), in time dependent manner in both cases. As showed in Fig. 11, there was a difference between the films prepared with AgNPs from hot-plate and AgNPs from MW approaches, and between low and medium CS loaded with NPs. The maximum release (about 1.4 ppm of Ag^+) was measured using nanocomposite developed by low CS and 120 μM of AgNPs from hot-plate (Fig. 11a). In line with this trend, using low CS films with AgNPs from MW at the higher concentration, we recorded about 1 ppm, so slightly lower than the films with AgNPs from hot-plate (Fig. 11b). Conversely, using neutral pH, the release was extremely low, even if the greater Ag^+ concentration was reported in Fig. 11c related to the CS films added with AgNPs from hot-plate at 120 μM (0.73 ppm) compared to the microwave's counterpart (Fig. 11d).

The difference in ppm between the acidic and neutral conditions can be explained by the greater H^+ concentration in the buffer that surround the CS films as also reported in [56]. In the first times, a fast release was observed up to 4 h; whereupon the increase of Ag^+ concentration became slower. This effect was more evident when pH value was 5.5.

Afterwards, in order to understand whether such concentrations could have *in vitro* toxic effects, we performed

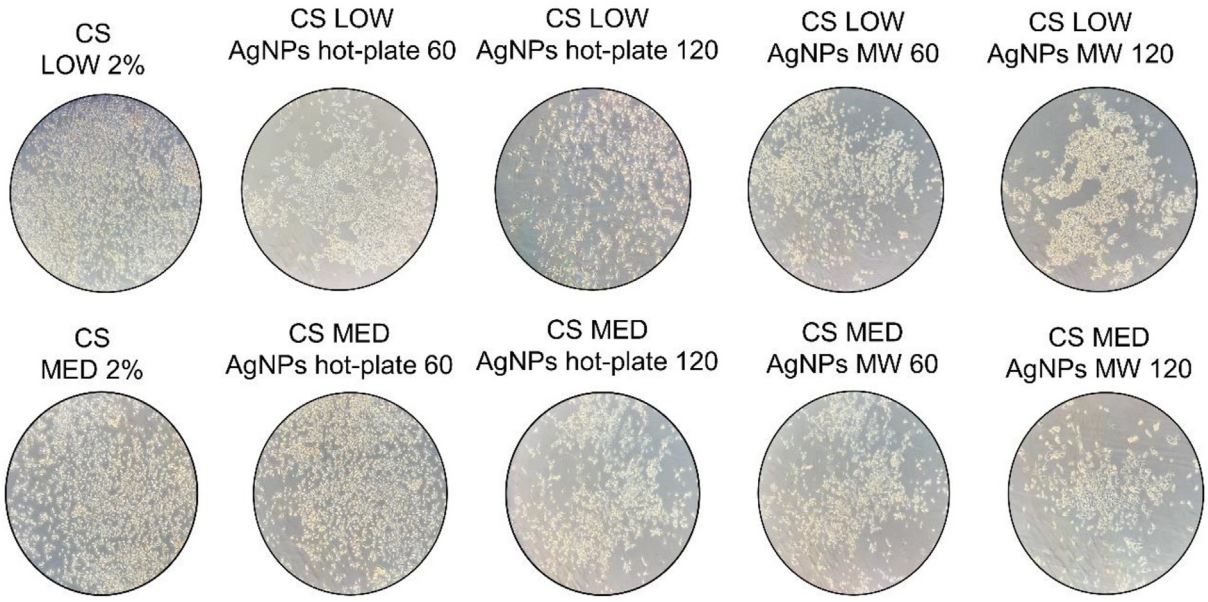

Fig. 13 – Optical microscope acquisitions of SH-SY5Y cells seeded on CS-based nanocomposite films.

viability test on neuroblastoma cells (SH-SY5Y); cells were exposed to the Ag^+ concentrations measured in the release experiments. At the same time, toxicity tests were carried out growing the cells on control and nanocomposite CS films, since these cells growth in adherence. The toxicity behavior is critical factor since the application is mainly in the food area and then, the oral ingestion of toxic elements can be a disadvantage limiting the application in this field.

For the toxicity assessment with Ag^+ ions, we referred to the values measured after 8 days of CS films incubation in acidic medium, since the higher values of ions release were recorded. At this time point, under these conditions (expressed in ppm) were reported in Table 4.

Subsequently, MTT test was performed, as shown in Fig. 12. The cells exposed to different Ag^+ concentrations did not show significant viability reduction after 48 h of exposure (Fig. 12a).

Growing cells on CS films, no mortality was recorded after 24 h, whereas, after 48 h decrease of cell viability was observed, which never reached more than 20% both using films with AgNPs from hot-plate (Fig. 12b) and AgNPs from MW (Fig. 12c).

The proliferation of cells on the CS films was also analyzed by using an optical microscope showing a general good biocompatibility of CS films for cells (Fig. 13). The images were acquired washing several times the films with PBS to eliminate any traces of cell culture medium. The morphology of the cells was maintained also using CS with high concentrations of AgNPs both from hot-plate and MW synthesis.

4. Conclusions

In this experimental work, we made CS films enriched with AgNPs obtained by two different synthetic techniques, both eco-friendly, using *Aloe Vera* leaves extract. We therefore added these NPs (final concentrations 60 μM and 120 μM) into the low and medium molecular weight CS polymer matrix.

The two molecular weights were compared since, having different polymeric chain lengths, different viscosity in solution was observed. Consequently, the dispersion of the AgNPs was different. The goal of the work was to develop films suitable for food packaging as alternative to commercial available plastics, which are toxic and difficult to recycle. We evaluated whether the addition of AgNPs could improve the chemical and physical properties of our films. The data presented in the paper allowed us to conclude the following.

- Addition of both AgNPs derived from hot-plate and MW synthesis in low and medium CS resulted in physico-chemical properties improvement of CS films.
- The addition of AgNPs derived from hot-plate induced the best protection from visible and near-infrared light, because they lend to the CS film a darker coloration than NPs derived from MW.
- Films enriched with AgNPs from MW were less sensitive to water incorporation, which means that the swelling ratio was more limited than CS having AgNPs derived from hot-plate. This phenomenon could be explained by better mixing within the polymer matrix being these nano-structures smaller and more colloidally stable. In addition, they showed greater thermal stability compared to the pure CS.
- Results related to the contact angle measurements showed that the addition of AgNPs achieved by MW in low CS caused an increase of the contact angle, i.e., hydrophobicity.
- Roughness measurements compared with contact angle values showed a proportional trend in the case of AgNPs addition from MW in CS. However, the addition of the two types of NPs induced an increase in roughness compared to the controls, which generally results in a more

hydrophobic surface. The friction coefficient measurements showed no significant differences from the control, making these films little prone to crack formation or other mechanical damage.
- Finally, the evaluation of Ag^+ release showed that only in the case of acidic pH condition, a minimal release measurable in terms of ppm of Ag^+ was detectable. Moreover, using the highest concentrations of released Ag^+ to incubate cells, no relevant mortality was evidenced. Same results were obtained by growing the cell line on the films supplemented with for 24 h and 48 h.
- Future goals will regard antibacterial tests on specific pathogens responsible of food contamination.

Author contributions

Conceptualization, V.D.M.; methodology, V.D.M., M.C., D. C, S.M, D.M., A.C., S.M, F.P; software, V.D.M., M.C.; validation, V.D.M.; formal analysis, V.D.M.; investigation, V.D.M. and M.C.; data curation, V.D.M.; writing—original draft preparation, V.D.M.; writing—review and editing, V.D.M., M.C., M.M. and R.R.; supervision, V.D.M. and R.R.; project administration, V.D.M. and R.R . All authors have read and agreed to the published version of the manuscript.

Data availability statement

The data presented in this study are available in this article.

Declaration of Competing Interest

The authors declare that they have no known competing financial interests or personal relationships that could have appeared to influence the work reported in this paper.

Acknowledgments

V.D.M. kindly acknowledges Programma Operativo Nazionale (PON) Ricerca e Innovazione 2014-2020-azione IV.6 “Contratti su tematiche green”-DM 1062/2021 for sponsoring her salary and work.

REFERENCES

[1] Shrivastava A. 1 - introduction to plastics engineering. In: Shrivastava A, editor. Introduction to plastics engineering. Plastics design library. William Andrew Publishing; 2018, ISBN 978-0-323-39500-7. p. 1–16.
[2] Alarifi IM. Chapter 2 - synthetic polymers. In: Alarifi IM, editor. Synthetic engineering materials and nanotechnology. Elsevier; 2022, ISBN 978-0-12-824001-4. p. 33–58.
[3] Jean-Paul. Lange managing plastic Waste—Sorting, recycling, disposal, and product redesign. ACS Sustain. Chem. 2021;9:5722–15738.
[4] Thompson RC, Moore CJ, Saal FSV, Swan SH. Plastics, the environment and human health: current consensus and future trends. Philos. Trans. R. Soc. B Biol. Sci. 2009;364:2153–66. https://doi.org/10.1098/rstb.2009.0053.
[5] Proshad R, Kormoker T, Islam MS, Haque MA, Rahman MM, Mithu MMR. Toxic effects of plastic on human health and environment : a consequences of health risk assessment in Bangladesh. Int J Health 2017;6:1. https://doi.org/10.14419/ijh.v6i1.8655.
[6] Evan S, Beach ZC, A PT. Green Chemistry: a design framework for sustainability. Energy Environ Sci 2009;2:1038. 1.
[7] Bradu P, Biswas A, Nair C, Patil M, Kannampuzha S, et al. Recent advances in green technology and Industrial Revolution 4.0 for a sustainable future. Environ Sci Pollut Res 2022. https://doi.org/10.1007/978-981-16-1823-9_19.
[8] Dziuba R, Kucharska M, Madej-Kiełbik L, Sulak K, W.-W M. Biopolymers and biomaterials for special applications within the context of the circular economy. Mater 2021;14(24):770.
[9] Baranwal J, Barse B, Fais A, Delogu GL, Kumar A. Biopolymer: a sustainable material for food and medical applications. Polymers 2022;14:1–22. https://doi.org/10.3390/polym14050983.
[10] Raschip, I.E., Fifere, N., Dinu, M.V. (2021). Polysaccharide-based materials as promising alternatives to synthetic-based plastics for food packaging applications. Bioplastics for Sustainable Development. Kuddus, M., Roohi Bioplastics Sustain. Dev. Springer, Singapore. https://link.springer.com/chapter/10.1007/978-981-16-1823-9_19 2021.
[11] Flórez M, Guerra-Rodríguez E, Cazón P, Vázquez M. Chitosan for food packaging: recent advances in active and intelligent films. Food Hydrocolloids 2022;124. https://doi.org/10.1016/j.foodhyd.2021.107328.
[12] Siripatrawan U, Harte BR. Physical properties and antioxidant activity of an active film from chitosan incorporated with green tea extract. Food Hydrocolloids 2010;24:770–5. https://doi.org/10.1016/j.foodhyd.2010.04.003.
[13] Abdul Khalil HPS, Chong EWN, Owolabi FAT, Asniza M, Tye YY, Rizal S, et al. Enhancement of basic properties of polysaccharide-based composites with organic and inorganic fillers: a review. J Appl Polym Sci 2019;136. https://doi.org/10.1002/app.47251.
[14] Othman SH. B bio-nanocomposite materials for food packaging applications: types of biopolymer and nano-sized filler. Agric Agric Sci Procedia 2014;2:296. –303.
[15] Rhim J-W, Park H-M, Ha C-S. Bio-nanocomposites for food packaging applications. Prog Polym Sci 2013;38:1629–52. https://doi.org/10.1016/j.progpolymsci.2013.05.008.
[16] Marra A, Silvestre C, Duraccio D, Cimmino S. Polylactic acid/zinc oxide biocomposite films for food packaging application. Int J Biol Macromol 2016;88:254–62. https://doi.org/10.1016/j.ijbiomac.2016.03.039.
[17] Pounraj S, Somu P, Paul S. Chitosan and graphene oxide hybrid nanocomposite film doped with silver nanoparticles efficiently prevents biofouling. Appl Surf Sci 2018;452:487–97. https://doi.org/10.1016/j.apsusc.2018.05.009.
[18] Gao H-X, He Z, Sun Q, He Q, Zeng W-C. A functional polysaccharide film forming by pectin, chitosan, and tea polyphenols. Carbohydr Polym 2019;215:1–7. https://doi.org/10.1016/j.carbpol.2019.03.029.
[19] Soltaninejad V, Maleki A. A green, and eco-friendly bionanocomposite film (poly(vinyl alcohol)/TiO2/chitosan/chlorophyll) by photocatalytic ability, and antibacterial activity under visible-light irradiation. J Photochem Photobiol Chem 2021;404:112906. https://doi.org/10.1016/j.jphotochem.2020.112906.

[20] De Matteis V,R,R. Toxicity assessment in the nanoparticle era. In: Cellular and molecular toxicology of Nanoparticles.Advances in experimental medicine and biology. Cham: Springer; 2018. p. 1–19.
[21] Ijaz I, Gilani E, Nazir A, Bukhari A. Detail review on chemical, physical and green synthesis, classification, characterizations and applications of nanoparticles. Green Chem Lett Rev 2020;13:59–81. https://doi.org/10.1080/17518253.2020.1802517.
[22] Iravani S. Green synthesis of metal nanoparticles using plants. Green Chem 2011;13:2638.
[23] De Matteis V, Rizzello L, Ingrosso C, Liatsi-Douvitsa E, De Giorgi ML, De Matteis G, R.R. Cultivar-dependent anticancer and antibacterial properties of silver nanoparticles synthesized using leaves of different olea europaea trees. Nanomaterials 209AD, 9, 1544.
[24] De Matteis V, Cascione MF, Toma CC, L S. Silver nanoparticles: synthetic routes, in vitro toxicity and theranostic applications for cancer disease. Nanomaterials 2018;8:1–23.
[25] Ahlawat KS, K B. Processing, food applications and safety of aloe vera products: a review. J Food Sci Technol 2011;48(5):525.
[26] Eshun K, He Q. Aloe vera: a valuable ingredient for the food, pharmaceutical and cosmetic industries—a review. Crit Rev Food Sci Nutr 2004;44:91–6. https://doi.org/10.1080/10408690490424694.
[27] Surjushe A, Vasani R, Saple DG. Aloe vera: a short review. Indian J Dermatol 2008;53:163. 16.
[28] López A, De Tangil MS, Vega-Orellana O, Ramírez AS, Rico M. Phenolic constituents, antioxidant and preliminary antimycoplasmic activities of leaf skin and flowers of aloe vera (L.) burm. F. (syn. A. barbadensis mill.) from the canary islands (Spain). Molecules 2013;18:4942–54. https://doi.org/10.3390/molecules18054942.
[29] Naidu R, Biswas B, Willett IR, Cribb J, Kumar Singh B, Paul Nathanail C, et al. Chemical pollution: a growing peril and potential catastrophic risk to humanity. Environ Int 2021;156:106616. https://doi.org/10.1016/j.envint.2021.106616.
[30] de Marco BA, Rechelo BS, Tótoli EG, Kogawa AC, Salgado HRN. Evolution of green chemistry and its multidimensional impacts: a review. Saudi Pharmaceut J 2019;27:1–8. https://doi.org/10.1016/j.jsps.2018.07.011.
[31] Surjushe A, Vasani R, S D. Aloe vera: a short review. Indian J Dermatol 2008;53:163–6.
[32] Jia Y, Jia J. Ultraviolet light absorption of an ophthalmic formulation. Nat Prod Commun 2009:13–5.
[33] Bayram, S.S.; Lindfors, K.; Blum, A.S. Tunable longitudinal modes in extended silver nanoparticle assemblies. 2016, 1219–1228, doi:10.3762/bjnano.7.113.
[34] Teixeira-costa BE. Chitosan as a valuable biomolecule from seafood industry waste in the design of green. Food Packaging 2021;1–19.
[35] Tiwary AK, Rana V. Cross-linked chitosan films : effect of cross-linking density on swelling parameters CROSS-LINKED CHITOSAN FILMS : effect of cross-linking density on swelling parameters. 2010.
[36] Mi F-L, Shyu S-S, Lee S-T, Wong T-B. Kinetic study of chitosan-tripolyphosphate complex reaction and acid-resistive properties of the chitosan-tripolyphosphate gel beads prepared by in-liquid curing method. J Polym Sci B Polym Phys 1999;37:1551–64.
[37] Croisier F, Jérôme C. Chitosan-based biomaterials for tissue engineering. Eur Polym J 2013;49:780–92. https://doi.org/10.1016/j.eurpolymj.2012.12.009.
[38] Lodge TP. Polymer chemistry. CRC Press; 2007.
[39] Aranaz I, Harris R, Navarro-García F, Heras A, Acosta N. Chitosan based films as supports for dual antimicrobial release. Carbohydr Polym 2016;146:402–10. https://doi.org/10.1016/j.carbpol.2016.03.064.
[40] Chudobova D, Nejdl L, Gumulec J, Krystofova O, Rodrigo MA, Kynicky J, et al. Complexes of silver(I) ions and silver phosphate nanoparticles with hyaluronic acid and/or chitosan as promising antimicrobial agents for vascular grafts. Int J Mol Sci 2013;14:13592–614.
[41] Mele MF, Garcı A, Paulraj M, Ca G. Semitransparent chitosan-TiO 2 nanotubes composite film for food package applications. 2010. https://doi.org/10.1002/app.
[42] Meiron TS, Saguy IS. Wetting properties of food packaging. Food Res Int 2007;40:653–9. https://doi.org/10.1016/j.foodres.2006.11.010.
[43] Abraham Marmur Soft contact: measurement and interpretation of contact angles. Soft Matter 2006;2:12–7.
[44] Douglas de Britto OBGA. Hydrophilic and morphological aspects of films based on quaternary salts of chitosan for edible applications. Packag. Technol. Sci. an Int. journal. 2010;23.
[45] Basavegowda N BK-H. Advances in functional biopolymer-based nanocomposites for active food packaging applications. Polym 2021;13(23):4198.
[46] Lavrič, G.; Oberlintner, A.; Filipova, I.; Novak, U.; Likozar, B.; Vrabič-Brodnjak, U. Functional nanocellulose, alginate and chitosan nanocomposites designed as active film packaging materials. Polym. 13, 2523.
[47] Salari M, Sowti Khiabani M, Rezaei Mokarram R, Ghanbarzadeh B, Samadi Kafil H. Development and evaluation of chitosan based active nanocomposite films containing bacterial cellulose nanocrystals and silver nanoparticles. Food Hydrocolloids 2018;84:414–23. https://doi.org/10.1016/j.foodhyd.2018.05.037.
[48] Bailey EJ, Winey KI. Dynamics of polymer segments, polymer chains, and nanoparticles in polymer nanocomposite melts: a review. Prog Polym Sci 2020;105:101242. https://doi.org/10.1016/j.progpolymsci.2020.101242.
[49] Pinto D, Amaro AM, Bernardo L. Experimental study on the surface properties of nanoalumina-filled epoxy resin nanocomposites oxide. Appl Sci 2020;10:733.
[50] Rath A, Mathesan S, Ghosh P. Nanomechanical characterization and molecular mechanism study of nanoparticle reinforced and cross-linked chitosan biopolymer. J Mech Behav Biomed Mater 2016;55:42–52. https://doi.org/10.1016/j.jmbbm.2015.10.005.
[51] Li F, Biagioni P, Bollani M, Maccagnan A, Piergiovanni L. Multi-functional coating of cellulose nanocrystals for flexible packaging applications. Cellulose 2013;20:2491–504.
[52] Ljevak, I.; Zjakić, I.; Banić, D. The variability of dynamic coefficient of friction material in flexible packaging. 31–38.
[53] Castro JI, Valencia-Llano CH, Zapata MEV, Restrepo YJ, Hernandez JHM, Navia-Porras DP, et al. Chitosan/polyvinyl alcohol/tea tree essential oil composite films for biomedical applications. Polymers 2021;13:1–21. https://doi.org/10.3390/polym13213753.
[54] Al-Sagheer F, Muslim S. Thermal and mechanical properties of chitosan/SiO2 hybrid composites. J Nanomater 2010;2010. https://doi.org/10.1155/2010/490679.
[55] Timur M, Pas A Synthesis. Characterization , swelling , and metal uptake studies of aryl cross-linked chitosan hydrogels. ACS Omega 2018:2–10. https://doi.org/10.1021/acsomega.8b01872.
[56] Kadam D, Momin B, Palamthodi S, L S. Physicochemical and functional properties of chitosan-based nano-composite films incorporated with biogenic silver nanoparticles. Carbohydr Polym 2019;1:124–32.